JVST A
Journal of Vacuum Science & Technology A

ARTICLE

avs.scitation.org/journal/jva

Scaling of atomic layer etching of SiO_2 in fluorocarbon plasmas: Transient etching and surface roughness

Cite as: J. Vac. Sci. Technol. A **39**, 033003 (2021); doi: 10.1116/6.0000941
Submitted: 21 January 2021 · Accepted: 2 March 2021 ·
Published Online: 16 March 2021

Xifeng Wang,[1,a)] Mingmei Wang,[2,b)] Peter Biolsi,[2,c)] and Mark J. Kushner[1,d)]

AFFILIATIONS

[1] Department of Electrical Engineering and Computer Science, University of Michigan, 1301 Beal Ave., Ann Arbor, Michigan 48109-2122
[2] TEL Technology Center, America, LLC, 255 Fuller Road, Suite 214, Albany, New York 12203

Note: This paper is part of the 2021 Special Topic Collection on Atomic Layer Etching (ALE).

[a)] **Electronic mail:** xifwang@umich.edu
[b)] **Electronic mail:** mingmei.wang@us.tel.com
[c)] **Electronic mail:** peter.biolsi@us.tel.com
[d)] **Author to whom correspondence should be addressed:** mjkush@umich.edu

ABSTRACT

Fabricating sub-10 nm microelectronics places plasma processing precision at atomic dimensions. Atomic layer etching (ALE) is a cyclic plasma process used in semiconductor fabrication that has the potential to remove a single layer of atoms during each cycle. In self-limiting ideal ALE, a single monolayer of a material is consistently removed in each cycle, typically expressed as EPC (etch per cycle). In plasma ALE of dielectrics, such as SiO_2 and Si_3N_4, using fluorocarbon gas mixtures, etching proceeds through deposition of a thin polymer layer and the process is not strictly self-terminating. As a result, EPC is highly process dependent and particularly sensitive to the thickness of the polymer layer. In this paper, results are discussed from a computational investigation of the ALE of SiO_2 on flat surfaces and in short trenches using capacitively coupled plasmas consisting of a deposition step (fluorocarbon plasma) and an etch step (argon plasma). We found that ALE performance is a delicate balance between deposition of polymer during the first half cycle and etching (with polymer removal) during the second half cycle. In the absence of complete removal of the overlying polymer in each cycle, ALE may be transient as the polymer thickness grows with each cycle with a reduction in EPC until the thickness is too large to enable further etching. Small and statistical amounts of polymer left from a previous cycle can produce statistical variation in polymer thickness on the next cycle, which in turn can lead to a spatially dependent EPC and ALE roughness. Based on synergy between T_i (sputtering time) and T_p (passivation time), dielectric ALE can be described as having three modes: deposition, roughening surface (transitioning to etch-stop), and smooth surface with steady-state EPC.

I. INTRODUCTION

As features in microelectronics devices shrink to sub-10 nm and the thickness of dielectric materials approaches a monolayer, plasma etching processes are being challenged by uniformity requirements and the difficult-to-minimize variability in plasma properties.[1–4] Advanced three-dimensional structures such as FinFETs and gate-all-around transistors[5] require high etching selectivity between the devices and hard mask structures. Smaller and thinner structures are more sensitive to surface defects caused by energetic ion bombardment during plasma etching, which can degrade or add variability to performance.[6–12]

Atomic layer etching (ALE) is a potential remedy to many of these challenges. ALE is a cyclic process that has, in principle, the ability to remove a monolayer of material per cycle. A typical plasma-based ALE process consists of two steps. The first is passivation typically performed with high fluxes of radicals and low fluxes of ions having low energies onto the wafer. During the passivation step, precursors chemically react with the substrate to generate a passivation layer, which has a lower threshold energy for chemical sputtering compared with the underlying material. The second step consists of low fluxes of radicals and high fluxes of ions having moderate energies. These ion fluxes are intended to remove the passivation layer without etching the underlying material.

Ideally both steps should be self-limited. The passivation step should self-terminate when the surface is fully passivated. The etching step should self-terminate when the passivation layer is removed. The former requires passivation chemistry that does not also involve deposition, such as halogen passivation of Si or Ge. When all surface sites are passivated by forming $SiCl_x$, for example, then further passivation is blocked. The latter requires careful control of the ion energy distribution (IED), with ions being energetic enough to chemically sputter the passivation but not energetic enough to physically sputter the underlying materials.[13–15] Additional requirements to achieve ideal conditions include lack of energetic ions during the passivation step that might chemically sputter the passivation and lack of radicals during the ion bombardment-etch step that would passivate newly exposed sites.

Plasma-based ALE has been investigated from the 1990s with an initial focus on silicon and GaAs using chlorine and bromine containing plasmas for passivation.[16–19] These systems are capable of having self-terminating steps and approaching ideal ALE results. Investigations have addressed the ideal aspects of ALE experimentally[20–22] and computationally.[23,24] Using an electron-cyclotron-resonance plasma system, Matsuura *et al.*[20] reported that EPC (etch per cycle) for Si ALE increased with chlorine plasma exposure time, saturating to a constant value when self-limited adsorption of chlorine was reached. This finding was confirmed by Park *et al.*[22] who reported that saturated EPC in ALE of Si could be obtained when the Ar^+ ion acceleration voltage was in the range of 70–90 V, preferentially etching the silicon chloride passivation while having low rates of sputtering of the underlying Si. The substrate temperature was reported as having an impact on EPC, demonstrated by modulating the temperature synchronously with the chlorine adsorption and $SiCl_x$ desorption steps.[21]

Although ALE of dielectrics has been demonstrated using halogen gases for passivation,[25] the plasma ALE of dielectrics differs from that of conductors dominantly in the passivation step. In ALE of conductors using halogen containing and nonpolymerizing gases, the passivation of the surface is self-limiting. In ALE of dielectrics, the passivation step is usually conducted using polymerizing fluorocarbon gases, for example, an Ar/C_4F_8 plasma.[26] The passivation of the surface consists of deposition of a fluorocarbon polymer (FCP) layer. The FCP layer consists of the passivated interface between the dielectric and the FCP, with additional FCP deposited on top of the interfacial passivation, sometimes referred to as selvedge. In principle, an arbitrarily thick FCP layer can be deposited during the passivation step. Since the FCP is the fuel used to chemically sputter the dielectric, etching can proceed for as long as there is polymer remaining on the surface and ions can penetrate the FCP to the SiO_2 interface to activate the etch. As a result, there is no intrinsic process that might limit the EPC to a single monolayer.

This lack of self-limiting passivation during plasma ALE of dielectrics presents several challenges in terms of added process variability. Computational and experimental investigations have shown that by controlling the thickness of the FCP during the deposition step and judicious choice of the fluorocarbon gas, controlled EPC can be achieved during the ion chemical sputtering step.[26–33] Substrate temperature is another ALE control mechanism that affects the thickness and composition of the FCP layer.[34] In conventional fluorocarbon plasma etching, this process is continuous and a steady-state FCP layer of up to a few nm is produced.

In fluorocarbon plasma ALE of dielectrics, the thickness of the FCP layer is critical to the selectivity between materials. Li *et al.* experimentally investigated FCP assisted ALE of Si_3N_4 and SiO_2 as used, for example, in etching of self-aligned contacts. This process requires high selectivity by preferentially etching SiO_2 compared to the Si_3N_4 stop-layer.[31] They concluded that highly selective SiO_2 to Si_3N_4 etching can be achieved by optimizing the ALE process parameters including low ion energies, short etching step length, and high FCP deposition per cycle to produce higher net rates of FCP deposition on Si_3N_4. Huard *et al.* computationally demonstrated that control of the FCP overlayer is critically important to high selectivity during the ALE of SiO_2 and Si_3N_4.[32] Wang *et al.* computationally and experimentally investigated ALE and selectivity of SiO_2 and Si_3N_4 in capacitively coupled plasmas (CCPs) sustained in fluorocarbon gas mixtures.[29] They found that controlling the thickness of the FCP, typically larger on Si_3N_4, was critical to controlling selectivity. Blocking or clogging of features due to excessive FCP deposition was found to be sensitive to mask topography and deposition time.

The control of the FCP layer thickness is challenging as there is a small window in which the FCP is thick enough to produce the desired EPC during the ion activation stage but not so thick that the polymer cannot be fully removed. Most plasma ALE systems use a fluorocarbon plasma for the deposition and an inert gas plasma, usually argon, for the ion activated etch step. An alternate procedure uses an Ar/C_4F_8 plasma for deposition and an oxygen plasma for the ion activation step.[35] The oxygen plasma can additionally be used to control the thickness of the FCP and to remove any residual carbon that might otherwise be left on the SiO_2 after the etch step.

Pranda *et al.* evaluated the ALE process parameters of ion energy, etch step length, FCP thickness, and precursor gas to maximize the selectivity of SiO_2 with respect to EUV photoresist (PR).[36] They found that a modified surface layer on the PR was formed by controlling argon ion bombardment during sputtering and the FCP layer during passivation. These parameters were then used to control the PR etch rate while the etching of SiO_2 was largely unaffected, thereby enabling a high SiO_2/PR etching selectivity.

Achieving selectivity between dielectric materials during fluorocarbon plasma ALE in large part requires controlling the relative thickness of the FCP on the respective materials.[10] However, other strategies to achieve selectivity during ALE includes the use of additives. Gasvoda *et al.*[37] demonstrated high ALE selectivity of Si_3N_4 compared to SiO_2 by using an intermediate step consisting of exposure to bis(dimethylamino) dimethylsilane $[(CH_3)_2Si[N(CH_3)_2]_2]$. This exposure places Si-CH_3 groups on the SiO_2, which react with the FCP deposition to produce an inhibiting layer that slows or terminates the ALE process.

Selective ALE of dielectrics can also be performed in nonfluorocarbon systems. For example, Cho *et al.* experimentally investigated the plasma ALE of SiO_2 using CF_4/NH_3 mixtures.[38] They found that an ammonium fluorosilicate layer was formed in a self-limiting manner and which could be removed by subsequent thermal treatment above 100 °C using a lamp. A self-limiting oxide removal rate of 2.7 nm/cycle was achieved. A similar self-limiting process was achieved using an NF_3/NH_3 plasma with a removal rate of 9.1 nm/cycle, attributed to the more efficient production of F atoms with NF_3 compared to CF_4.

Although emphasis in ALE of dielectrics has focused on SiO_2 and Si_3N_4, ALE of other dielectrics has also been investigated. Lin *et al.* experimentally investigated the selective ALE of HfO_2 over Si using inductively coupled plasmas sustained in CH_4/CHF_3 and CH_4/C_4F_8 mixtures.[33] They found that CH_4/C_4F_8 mixtures produced a comparable FCP thickness on both HfO_2 and Si during the deposition step. In contrast, a CH_4/CHF_3 mixture deposited a FCP film on Si, while the HfO_2 surface was fluorinated with a negligible overlayer of FCP. Based on these trends, selective removal of HfO_2 over Si was achieved using CH_4/CHF_3 mixtures.

In this paper, results are discussed from a computational investigation of the plasma ALE of SiO_2 using capacitively coupled plasma (CCP) sources. The passivation step was performed using an $Ar/C_4F_8/O_2$ gas mixture and the chemical sputtering step was performed using an argon plasma. Parametric studies were performed while varying bias power, gas mixture, and length of the passivation and etch steps. We found that EPC is sensitive to the thickness of the FCP layer in that a thicker polymer layer will limit the ability for ions to penetrate through the polymer and passivation layers to chemically sputter the dielectric leading to lower EPC. The FCP thickness can be controlled by changing the passivation time, T_p. magnitude of polymerizing fluxes by gas mixture and bias power. That said, longer ion activation time, T_i, enables thicker FCP to be utilized. Small amounts of statistically distributed polymer left from a previous cycle can produce a spatially dependent FCP thickness, which leads to roughening of the etched surface. ALE of dielectrics can be described as having three modes: deposition, transient etching with a roughening surface (transitioning to an etch-stop), and smooth surface with steady-state EPC. The occurrence of these modes depends on a synergy between T_i and T_p.

The reactor and feature scale models used in this investigation are described in Sec. II. The dual-frequency CCP source, sustained in $Ar/C_4F_8/O_2$ and Ar, is described in Sec III. Based on blanket etching of SiO_2, scaling of ALE was investigated by changing the passivation time, sputtering time, and fluorocarbon gas ratio, and those results are discussed in Sec. IV. Scaling of ALE in short trenches is discussed in Sec. V. Concluding remarks are in Sec. VI.

II. DESCRIPTION OF THE MODELS

The reactor scale model used in this investigation is the two-dimensional Hybrid Plasma Equipment Model (HPEM), which has been described in detail previously.[39] The HPEM is a kinetic-fluid hydrodynamics model consisting of separate modules that address different physical phenomena. The major modules used in this investigation are as follows. The Fluid Kinetics Poisson Module provides densities, fluxes, and temperatures of all gas phase species through solution of continuity, momentum, and energy equations. Poisson's equation is solved for the electrostatic potential. An electron energy conservation equation is implicitly integrated to provide the electron temperature or mean electron energy. Electron impact rate coefficients and transport coefficients are then selected based on stationary solutions of Boltzmann's equation for the electron energy distribution. Transport of sheath accelerated secondary electrons is represented using a Monte Carlo simulation in the Electron Energy Transport Module. The Surface Kinetics Module employs a multilayer site balance model on surfaces in contact with the plasma to update boundary conditions for the plasma fluxes to surfaces. The Plasma Chemistry Monte Carlo Module is used to provide energy and angular distributions (EADs) of neutral species and ions onto the wafer surface. These modules are coupled spatiotemporally using time slicing and acceleration processes with time integration over hundreds to thousands of radio frequency (RF) cycles to achieve a quasisteady state.

The feature scale modeling of the wafer surface was performed using the Monte Carlo Feature Profile Model (MCFPM) described in Ref. 32. The model is based on a 3D Cartesian mesh containing voxels (cubic numerical cells) with each voxel representing a type of solid material. Gas phase species incident onto the wafer surface are treated as Monte Carlo pseudoparticles with fluxes and initial choices of angle and energy being obtained from the HPEM. The trajectories of the pseudoparticles are tracked until they strike a surface, at which time they physically or chemically react with the solid material, resulting in the material cell being removed or added to etch or deposit materials. The initial particle is deposited, implanted, or reflected. To model the cyclic ALE process, two separate HPEM calculations were performed for the passivation step and the chemical sputtering step, each providing a separate set of fluxes and EADs. During simulation of an ALE process using the MCFPM, reactants are alternately chosen from these two sets of fluxes and EADs. The gas pump-out and gas injection periods are not addressed in the MCFPM simulations.

The gas phase chemical mechanism is based on the work of Vasenkov *et al.*[40] The plasma gas phase species considered in this study are Ar, $Ar(1s_2)$, $Ar(1s_3)$, $Ar(1s_4)$, $Ar(1s_5)$, Ar(4p), Ar(4d), Ar^+, C_4F_8, C_4F_7, C_3F_7, C_3F_6, C_3F_5, C_2F_6, C_2F_4, C_2F_3, CF_4, CF_3, CF_2, CF, C, COF_2, COF, CO, SiF_4, SiF_3, SiF_2, O_2, O_2^*, O, O^*, F, F_2, FO, Ar^+, $C_4F_8^+$, $C_4F_7^+$, $C_3F_7^+$, $C_3F_5^+$, $C_2F_4^+$, $C_2F_3^+$, CF_3^+, CF_2^+, CF^+, F^+, O_2^+, O^+, CF_3^-, F^-, O^-, and electrons. All of these species are included in the mechanism for the passivation step using $Ar/C_4F_8/O_2$ gas mixtures. For the chemical sputtering step, only the Ar species and electrons were included. That is, we did not include a C_xF_y impurity. Only F, O, and C_xF_y ($x \leq 2$, $y \leq 2$) neutrals are considered for chemical etching and passivation during step 1. Recipes for passivation during ALE of dielectrics do not require O_2, as in conventional continuous dielectric plasma etching where polymer etching by O_2 dissociation products is used to regulate the polymer thickness. O_2 is included here so that comparisons can be made to continuous etching. The consequence of including O_2 in the passivation gas mixture would be somewhat thinner FCP layers than a mixture without O_2.

III. REACTOR SCALE PROPERTIES: DUAL-FREQUENCY CAPACITIVELY COUPLED PLASMA

The geometry of the capacitively coupled, DC-augmented plasma reactor used in this investigation is shown in Fig. 1.

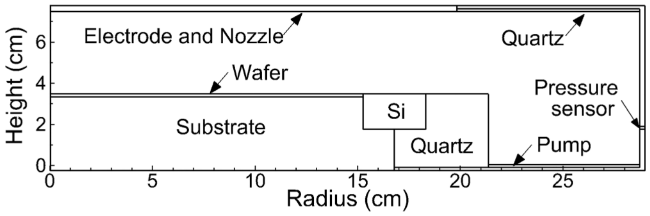

FIG. 1. Schematic of the reactor used in the model—a dual-frequency CCP with 10 and 50 MHz applied on the bottom electrode. A −500 V DC bias is added to the top electrode with the reactor walls being grounded.

The cylindrically symmetric reactor has a RF biased substrate holding a 30 cm diameter wafer. The wafer is surrounded by a focus ring consisting of silicon and quartz annuli. Gas is pumped from an annulus surrounding the substrate. The top electrode also serves as a gas showerhead and is surrounded by a quartz ring. All other surfaces are grounded metal. The wafer-to-top electrode spacing is 3.5 cm. All materials in contact with the plasma were maintained at a temperature of 293 K except the showerhead whose temperature was 333 K. Secondary electron emission by ion impact occurred with the following probabilities: wafer, 0.15; Si focus ring, 0.1; quartz focus ring, 0.05; outer chamber wall, 0.02; and top electrode, 0.15. Excited states of argon produced secondary electron emission on all surfaces with a probability of 0.01.

The ALE cycle consisted of two steps—fluorocarbon plasma passivation followed by argon plasma chemical sputtering. Both steps were performed in the same reactor. During the deposition step, the gas mixture for the base case was $Ar/C_4F_8/O_2 = 95/4/1$ with a total flow rate of 800 SCCM. The pump rate was adjusted to maintain a constant pressure of 25 mTorr. The top electrode was powered with a DC bias. The lower electrode was powered with an RF source at 50 MHz whose voltage amplitude was adjusted to deliver a specified power. For the base case, the 50 MHz power was 100 W and the DC power was 75 W. The self-DC bias on the substrate was −25 V.

The chemical sputtering step was performed in pure argon having a flow rate of 800 SCCM and pressure of 25 mTorr. As with the deposition step, the top electrode was powered with a DC −500 V bias. The lower electrode was powered with a dual-frequency RF source at 10 and 50 MHz whose voltage amplitudes were adjusted to deliver specified powers. For the base case, the 50 MHz power was 100 W and the 10 MHz power was 50 W. The DC power from the top electrode was 30 W and the self-DC bias on the substrate was −69 V.

Time averaged electron density n_e during step 1 (deposition) and step 2 (chemical sputtering) for the base case are shown in Fig. 2. During the deposition step, the −500 V DC bias on the top electrode produces a sheath with thickness of 1 cm with an electron density at midgap of $2.6 \times 10^9\,cm^{-3}$, sustained by a bulk electron temperature of 3.5–5 eV. During the sputtering step, the maximum electron density is $3.5 \times 10^{10}\,cm^{-3}$ and electron temperature is 3.2 eV at the edge of the wafer. Fluxes of the major radicals and ions incident onto the wafer during step 1 using the $Ar/C_4F_8/O_2$ plasma and during the sputtering step 2 are listed in Fig. 2. Radical fluxes are dominated by C_2F_4 ($2.3 \times 10^{16}\,cm^{-2}\,s^{-1}$) due to the initial dissociation of C_4F_8. The relatively stable steric structure of C_2F_4 results in having a small impact on passivation. The major deposition precursors are the CF_3, CF_2, and CF radicals with fluxes of 6.2×10^{15}, 1.9×10^{15}, and $1.3 \times 10^{15}\,cm^{-2}\,s^{-1}$. Since the reactivity of these radicals scales with the number of dangling bonds, their contributions to deposition are approximately the same. The smaller fluxes of C_2F_3 ($9.5 \times 10^{13}\,cm^{-2}\,s^{-1}$) and C_2F_5 ($1.4 \times 10^{12}\,cm^{-2}\,s^{-1}$) also make contributions to FCP deposition. By contrast, F and O with fluxes of 2.2×10^{15} and $2.6 \times 10^{15}\,cm^{-2}\,s^{-1}$ will consume polymer during the passivation step to control the thickness of the FCP layer. Ion fluxes are 1–2 orders lower than the fluxes of radicals. Ar^+ has the highest flux, $3.1 \times 10^{14}\,cm^{-2}\,s^{-1}$, followed by $C_xF_y^+$ fluxes ranging from 10^{12} to $10^{14}\,cm^{-2}\,s^{-1}$.

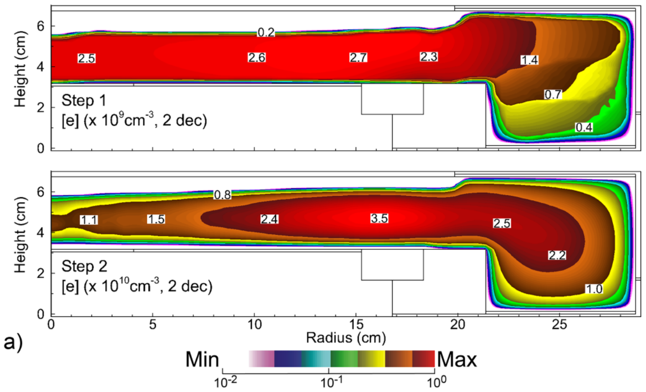

Step 1 Fluxes ($cm^{-2}s^{-1}$)					
Ar^+	3.1×10^{14}	CF_2^+	5.2×10^{12}	CF_2	1.9×10^{15}
$C_2F_4^+$	1.6×10^{14}	C_2F_4	2.4×10^{16}	CF	1.3×10^{15}
$C_2F_5^+$	1.6×10^{14}	CF_3	6.2×10^{15}	C_3F_7	5.4×10^{14}
CF^+	2.9×10^{13}	O	2.6×10^{15}	Step 2 Flux ($cm^{-2}s^{-1}$)	
CF_3^+	2.2×10^{13}	F	2.2×10^{15}	Ar^+	2.2×10^{15}

b)

FIG. 2. Time averaged plasma properties for the base case for step 1 [$Ar/C_4F_8/O_2 = 500/20/5$, 800 SCCM, 25 mTorr, 50 MHz, 100 W) and step 2 (Ar, 800 SCCM, 25 mTorr, 50/10 MHz = 100/50 W). (a) Electron density and (b) reactive fluxes to the substrate.

Ion energy and angular distributions (IEADs) and IEDs incident onto the wafer for all positive ions for step 1 (passivation) and step 2 (etching) are shown in Fig. 3. Ions during step 1 have energies up to 60 eV with an angular spread of ±15°. Even though some polymer can be sputtered with this range of ion energies, and there is some etching by oxygen atoms, the high ratio of the fluorocarbon radical flux to the ion flux results in net deposition. Since the energies of these ions are less than 60 eV, lower than the ion sputtering threshold energy of SiO_2 at about 70 eV,[41] the ions have little impact on material sputtering. The flux of Ar^+ during step 2 has a maximum energy of 130 eV with an angular spread of ±10°. This range of ion energies is able to penetrate through up to a few nm of FCP and still have energy above the threshold to remove the interfacial $SiO_2C_xF_y$ complex while not having a large rate of physical sputtering of SiO_2.

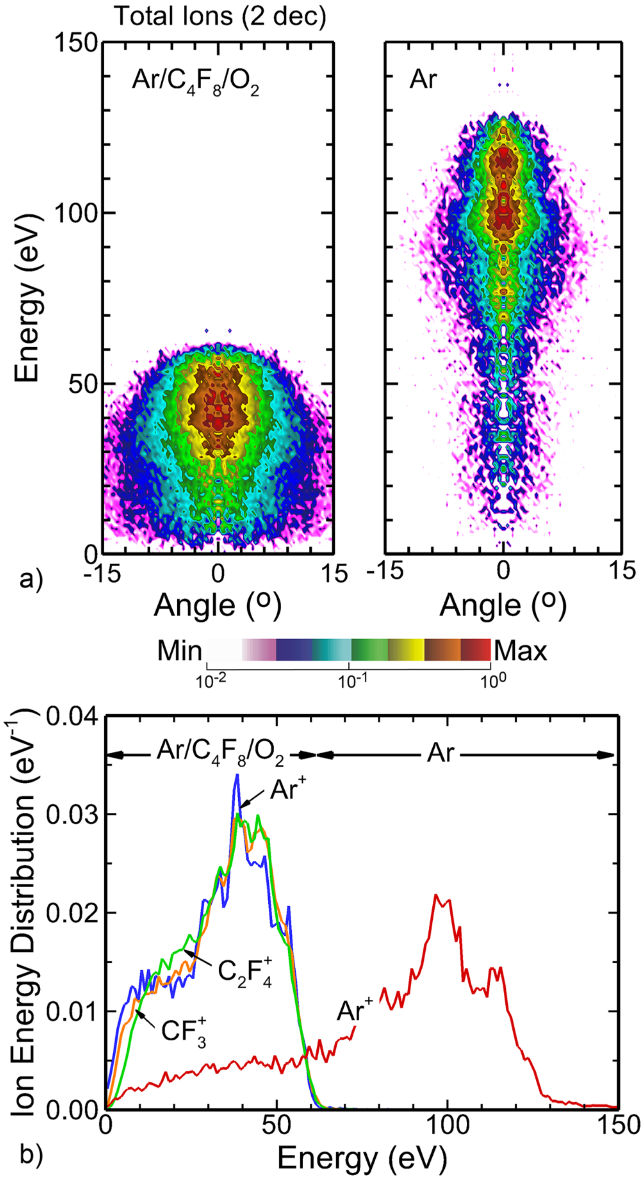

FIG. 3. Properties of positive ions incident onto the wafer for steps 1 and 2. (a) IEAD of all positive ions plotted on a two-decade log scale and (c) IED of selected positive ions. Operating conditions for step 1 are Ar/C_4F_8/O_2 = 500/20/5, 800 SCCM, 25 mTorr, 50 MHz, 100 W. For step 2, operating conditions are Ar, 800 SCCM, 25 mTorr, 50/10 MHz = 100/50 W.

IV. SCALING OF BLANKET ALE OF SiO_2

A. Surface reaction mechanism for ALE of SiO_2 in fluorocarbon plasmas

The surface reaction mechanism for ALE of SiO_2 in fluorocarbon plasmas used in this investigation is essentially the same as discussed by Huard *et al.*[32] The chemical sputtering mechanism begins with CF_x radicals adsorbing on SiO_2 to form an interfacial complex $SiO_2C_xF_y$, often called the selvedge layer,

$$SiO_2(s) + CF_x(g) \rightarrow SiO_2C_xF_y(s). \tag{1}$$

An FCP layer is then deposited on top of the interfacial complex (selvedge) dominantly by CF_x radicals. Sputtering of the FCP occurs by ion bombardment and or by hot neutrals that result from ions reflecting from and neutralizing on surfaces. Etching of the FCP also occurs by O atoms. With the exception of the neutralization process, hot neutrals participate in the same reactions as their ion counterparts. (In the following discussion, the term *ion* should be interpreted as *ions and hot neutrals.*) Ion penetration through the FCP layer to the interfacial complex activates the etching process producing COF_x and SiF_x etch products. Depending on the ion energy, the chemical sputtering process will occur in a single step (high energy ions) or a sequence of steps, which individually liberates COF_x and SiF_x. Exposed Si sites are fluorinated by F atoms either directly from the plasma or diffusing through the FCP layer. Low energy ions can activate the FCP by producing free radical sites with higher probabilities for deposition and are subject to etching by F atoms. Incident CF_x radicals first physisorb on the interfacial complex and on the FCP and diffuse on the surface before chemically bonding. The sticking coefficients for CF_x radicals depend on the material and the activation of that material. Sticking on SiO_2 to form the interfacial complex has a probability of 0.2, and sticking to the interfacial complex to deposit FCP has the same probability. Sticking of CF_x to nonactivated FCP has a probability of 0.01 and to activated polymer has a probability of 0.03. Sticking of CF_x to exposed Si sites has a probability of 0.2.

To simplify the surface reaction mechanism, only a single CF_x species was included in these simulations. To convert the fluxes of the many C_xF_y species in the reactor scale mechanism to this single species in the surface mechanism, the reactivity of the fluxes was scaled by the number of dangling bonds in the radical, while accounting for steric factors. The flux of the CF_x radical in the surface mechanism was scaled as

$$\begin{aligned}\phi(CF_x) = 1.5 \times \phi(CF) + \phi(CF_2) + 0.5 \times \phi(CF_3) + 0.3\\ \times \phi(C_2F_4 + C_2F_3 + C_2F_5).\end{aligned} \tag{2}$$

In addition to the reactions discussed by Huard *et al.*,[32] direct physical sputtering of polymer and $SiO_2(s)$ by ions and hot neutrals was included in the mechanism. Energetic ions I^+ will directly sputter the overlying polymer P(s), interfacial complex $SiO_2C_xF_y(s)$ and underlying $SiO_2(s)$

$$P(s) + I^+ \rightarrow CF_2 + I \qquad (\varepsilon_{th} = 30\ \text{eV}), \tag{3a}$$

$$SiO_2C_xF_y(s) + I^+ \rightarrow SiF + CO_2 + I \qquad (\varepsilon_{th} = 50\ \text{eV}), \tag{3b}$$

$$SiO_2(s) + I^+ \rightarrow SiO_2 + I \qquad (\varepsilon_{th} = 70\ \text{eV}). \tag{3c}$$

The directly sputtered $SiO_2(s)$ and $SiO_2C_xF_y(s)$ leave bare sites $SiO_2(s)$, which will be passivated by either overlying FCP or during the next ALE cycle.

B. Blanket ALE of SiO$_2$

The scaling of blanket ALE of SiO$_2$ was first investigated. (The term blanket refers to a flat, unpatterned surface.) The computational domain was a 40 by 60 nm^2 SiO$_2$ film that is initially 20 nm thick. The computational cubic voxels were 0.5 nm on a side. Periodic boundary conditions were applied for both gas phase and surface species in the lateral directions. Gas phase particles moving upward through the top boundary were removed from the simulation. A measure of the ALE process in the following discussion will be the height of the top of the surface, which is an average over a 7 by 7 nm^2 patch in the center of the feature. Changes in that height then indicate net etching or deposition.

The height of the SiO$_2$ film for three conditions are compared in Fig. 4: cw (continuous wave) exposure of the surface to only the passivation plasma (step 1), cw exposure to only the etching plasma (step 2), and the ALE process (sequentially repeating steps 1 and 2). For ALE, the passivation time for step 1 was $T_p = 5$ s and the chemical sputtering time for step 2 was $T_i = 20$ s. With only exposure to the passivation plasma, the thickness of the FCP layer on the surface of the SiO$_2$ grows to about 0.9 nm after 25 s, gradually increasing to about 1.5 nm after 200 s. This relatively slow rate of polymer growth is partly due to the oxygen in the gas mixture that etches the polymer. Exposure to only the chemical sputtering plasma produces physical sputtering of less than 1 nm.

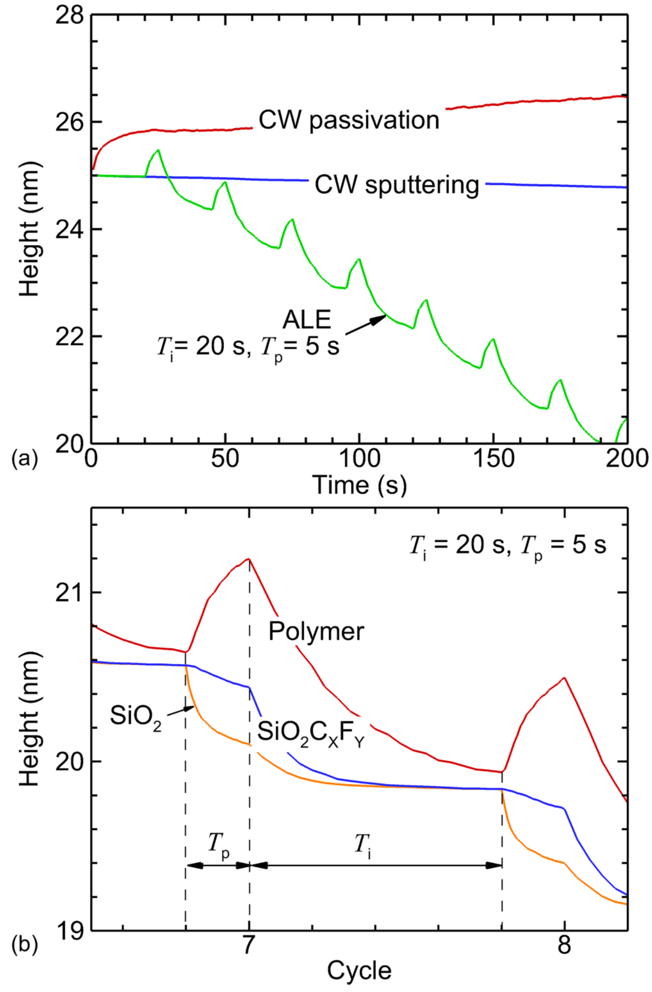

FIG. 4. Properties for blanket ALE of SiO$_2$. (a) Heights of the top surface for cw passivation, cw sputtering, and cyclic ALE with $T_i = 20$ s and $T_p = 5$ s. (b) Height of polymer, passivating SiO$_2$C$_x$F$_y$, and SiO$_2$ within an ALE cycle.

The sequential ALE process produces net etching of 0.7 nm per cycle. The ALE process is a delicate balance between polymer deposition during the first half of the cycle and etching (with polymer removal) during the second half. The etch front heights of the polymer, passivation layer SiO$_2$C$_x$F$_y$, and SiO$_2$over one ALE cycle are shown in Fig. 4(b). For an efficient and fully limiting ALE process, the FCP and the interfacial complex at the beginning of the passivation step should have been fully removed during the prior etch cycle. Here, the passivation step begins with a thin FCP layer remaining from the etch step. During the passivation step, the incident CF$_x$ flux forms the interfacial complex, converting the top layer of SiO$_2$ to SiO$_2$C$_x$F$_y$. Once the interfacial layer is formed, the CF$_x$ radicals then produce an overlayer of FCP. During this process, there is slight chemical etching of the SiO$_2$C$_x$F$_y$ due to ion penetration through the FCP. At the end of the passivation step of $T_p = 5$ s, the combination of the interfacial SiO$_2$C$_x$F$_y$ and FCP produces a 1.2 nm thick layer on top of the SiO$_2$. During the etch step of $T_i = 20$ s, ion penetration through the FCP layer first removes the existing SiO$_2$C$_x$F$_y$ layer and second removes SiO$_2$C$_x$F$_y$ being regenerated by the overlying FCP. The etch process terminates after about 10 s with a thin FCP layer remaining.

The thin remaining FCP is counterintuitive as one would expect chemical sputtering to continue as long as there is any FCP remaining—and that expectation is true. The heights shown in Fig. 4 are averages over a finite extent of the film. Some sites in that averaging domain are bare silicon, and some sites have a single layer of FCP. These trends are shown by the blanket SiO$_2$ profiles after 5 s of passivation and 20 s sputtering for the seventh cycle in Fig. 5(a). At the end of step 1, the passivation covers the entire SiO$_2$ film; however, the local coverage is statistical. That is, some sites have a statistically thicker FCP than others. With a FCP flux of 1.4×10^{16} cm^{-2} s^{-1}, deposition time of 5 s, site density of 10^{15} cm^{-2}, and sticking coefficient of 0.2, the average number of sticking radicals per site per cycle is about 14. This small number of sticking radicals produces a statistical random variation in thickness of 25%. This random FCP thickness is somewhat mediated by diffusion of the FCP precursors over the surface, but it is not reduced to zero. So the thickness of the nm deep FCP layer is inherently statistical. During the 20 s chemical sputtering step, each site is struck by about ten ions, which has about a 30% statistical variation. Combined with the statistical FCP thickness, at the end of the chemical sputtering period, there are patches of the film that are bare SiO$_2$ and patches of the film that retain a FCP overlayer. As the residual FCP is removed, it becomes statistically less likely to remove the isolated patches of FCP. This leaves a statistically rough surface at the beginning of the next deposition step. This roughness is best seen by the side view of the passivated surface.

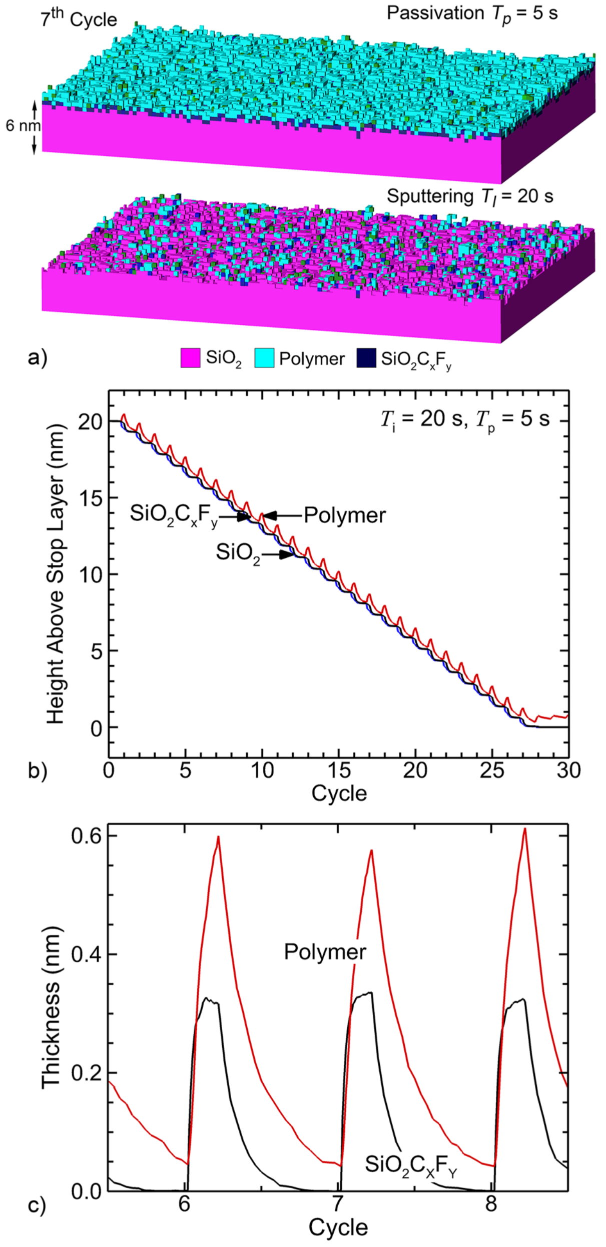

FIG. 5. Properties of ALE of blanket SiO_2 with passivation $T_p = 5$ s and sputtering $T_i = 20$ s. (a) Surface properties of SiO_2 after passivation for the seventh ALE cycle. (b) Heights of polymer, $SiO_2C_xF_y$, and SiO_2 during continuous ALE until reaching the stop-layer. (c) Height (or thickness) of the polymer and $SiO_2C_xF_y$ above the underlying SiO_2 during several ALE cycles.

For these conditions, the polymerizing flux during step 1 and chemical sputtering flux during step 2 are well balanced, resulting in a continuous periodic etch of about 0.8 nm/cycle, as shown in Fig. 5(b). The etch continues until reaching the underlying stop-layer. The deposition of polymer, production of the interfacial complex, and their removal are replicated cycle-to-cycle. For example, the heights or thickness of the selvedge layer and polymer above the underlying SiO_2 are shown in Fig. 5(c) for several ALE cycles. Typical experimental values for the FCP polymer layer are 0.5–1 nm, which results in an EPC of up to 0.5–0.8 nm/cycle.[28,31]

EPC as a function of step 1 passivation time T_p are shown in Fig. 6(a) for $T_i = 20$ s, while multiplying the flux of polymerizing radicals by factors of 1–5. For short passivation times, the higher fluxes of fluorocarbon radicals enable larger EPC as a thicker FCP layer provides more fuel for the etch. However, this advantage is quickly lost with increasing T_p—the polymer incrementally increases in thickness until an etch-stop results.

To align with the EPC measured in experiments, the fluorocarbon radical flux from the base case was increased by a factor of 3. (The experiments were performed in a proprietary geometry that could not be replicated here, and so comparisons are intended to be qualitative.) EPC as a function of passivation time T_P for different values of step 2 chemical sputtering time T_i are shown in Fig. 6(b) for this value of fluorocarbon flux. With increasing T_p, the overlying FCP layer increases in thickness, which potentially provides more precursors for etching, which should increase EPC. To achieve the higher EPC, two conditions must be met. First, T_i must be long enough to consume the overlying FCP. Second, there must be little residual FCP left at the end of step 2. This trend is shown by the EPC for $T_i = 20$ s. Up to a passivation time of $T_p = 7$ s, T_i is long enough to consume the additional FCP, which then produces a larger EPC. For $T_p > 7$ s, the thicker FCP reduces the ion energy reaching the interface, which then decreases the EPC and increases the residual FCP left at the end of step 2. With $T_p > 15$ s, the residual FCP layer increases from cycle-to-cycle until the FCP at the end of step 1 is too thick to enable ion penetration. At this point, net etching stops and the system transitions to net deposition.

The same trends occur for smaller values of T_i. However, with the shorter period of chemical sputtering, thicker FCP layers cannot be consumed and more residual FCP is left at the end of Step 2. The maximum EPC then occurs with a shorter T_p (thinner FCP layer) and the transition to net deposition occurs at shorter T_p.

The trends predicted by the model are corroborated by experiments performed for similar process conditions. The experiment data are averages of 16 points at a radius of 10 cm on a blanket 30 cm, SiO_2 covered wafer after 15 ALE cycles. The experimental results for EPC are shown in Fig. 6(c) as a function of passivation time T_p for different values of chemical sputtering time T_i. Similar to the computed results, large values of T_i are able to consume the FCP that results from longer deposition times T_p producing an increase in EPC As T_i decreases, the maximum EPC decreases (less able to consume the FCP) and the maximum EPC occurs at a shorter T_p.

Both the EPC and the morphology of the film are functions of both T_p and T_i. EPCs for different sputtering times $T_i = 1$, 3, 5, 10, and 20 s as a function of passivation time are shown in Fig. 7(a). The EPC for sputtering times T_i longer than 10 s initially increase prior to saturating to a constant value with increasing T_p. The asymptotic EPCs are 1.1 nm/cycle for $T_i = 20$ s and 0.9 nm/cycle for $T_i = 10$ s. Longer passivation times T_p generally produce thicker polymer layers. Provided the thickness of FCP layer is below the penetration distance of the incident ions during the etch step, the

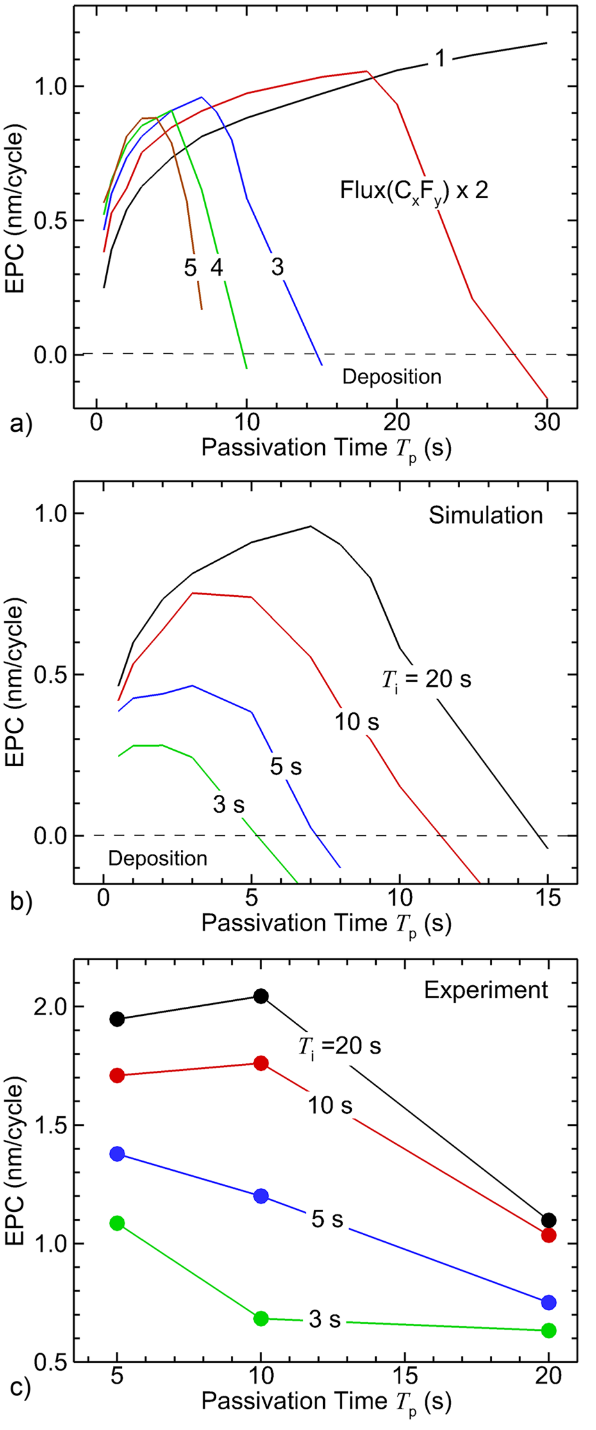

FIG. 6. EPC for ALE as a function of passivation time T_p. (a) EPC for $T_i = 20$ s while varying the magnitude of the polymerizing C_xF_y flux incident onto the substrate. The base case flux was multiplied by factors of 1–5. (b) EPC for $T_i = 3$, 5, 10, and 20 s with the base case polymerizing flux increased by a factor of 3. (c) Experimental values for EPC for conditions similar to those used for (b).

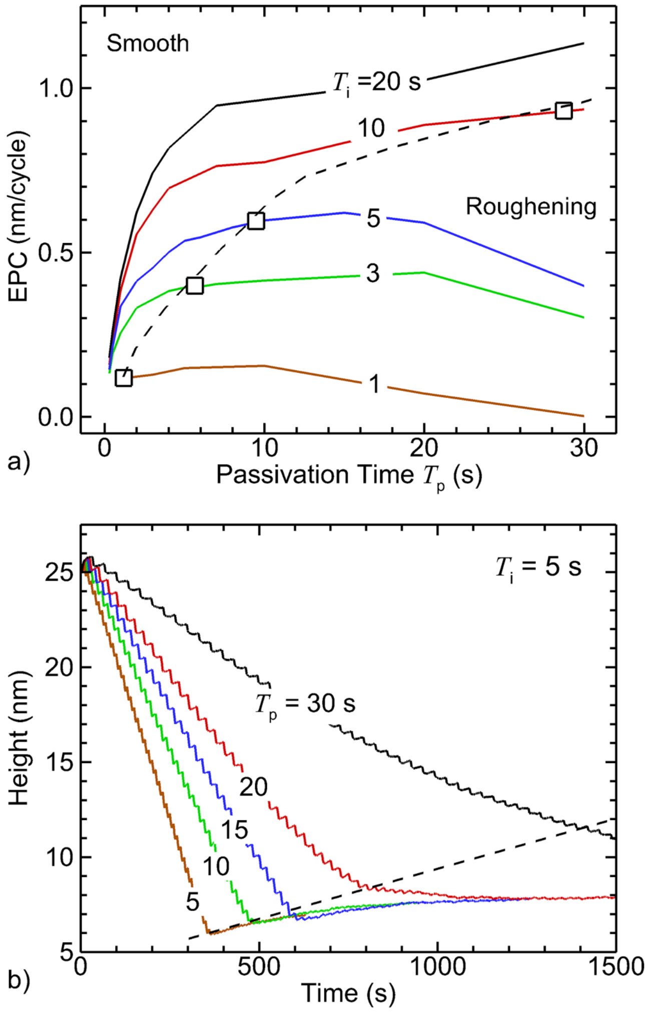

FIG. 7. ALE properties for different passivation times. (a) EPC as a function of passivation time T_p for $T_i = 1$, 3, 5, 10, and 20 s. The symbol on each curve is the transition between smooth continuous etching (lower T_p) and roughening surfaces (higher T_p). (b) Etch front height as a function of time with $T_i = 5$ s for passivation times of $T_p = 5$, 10, 15, 20, and 30 s.

thicker FCP layer provides more precursors for etching. In order to fully utilize the FCP, a critically long etch step T_i is required. For $T_i = 1$ s, the EPC = 0.05–0.12 nm/cycle for short T_p where the FCP is thin. However for thicker FCP, the short sputtering time is insufficient to remove enough polymer to prevent gradual thickening of the FCP. The end result is a cessation of etching at large T_P. With increasing T_i, a thicker FCP can be consumed, enabling an increase in EPC with increasing T_p. Predictions for EPC are in alignment with experiments in similar systems.[28,31,42]

For a given T_i, there is an FCP thickness above which the polymer can no longer be fully utilized, at which time the EPC saturates or decreases with increasing T_p. That is, for a given T_i, there is a passivation time T_p below which EPC is constant and above which the EPC decreases cycle-to-cycle. With the FCP not being fully removed from the previous cycle, the thickness of the FCP increases cycle-to-cycle, eventually reaching a thickness that produces an etch-stop. A similar behavior was observed by Pranda *et al.*[36] The demarcation between pulse-periodic continuous etching and a transition to an etch-stop is shown by the dotted line in Fig. 7(a). These trends are illustrated by the heights of the etch fronts for different passivation times T_p for a sputtering time of $T_i = 5$ s shown in Fig. 7(b). The height of 5 nm corresponds to the hard stop-layer under the SiO_2. For $T_p = 5$ s, quasicontinuous etching is able to clear the feature to the stop-layer, at which time a quasiconstant thickness FCP is formed. For $T_p > 5$ s, there is a slower and decreasing EPC produced by a thickening FCP, which results in an etch-stop prior to reaching the hard stop-layer.

The demarcation between continuous EPC and transition to an etch-stop also is a demarcation between smooth and rough surfaces. For example, etch profiles are shown in Fig. 8 for $T_i = 5$ s and $T_p = 5$ s after the 13th, 25th, and 36th cycles. Surfaces are also shown for $T_p = 20$ s after the 13th, 20th, and 30th cycles. With $T_p = 5$ s, SiO_2 is uniformly etched with a constant EPC. For each cycle, the FCP is nearly fully removed, leaving a nearly bare SiO_2 surface for the next deposition cycle. A constant EPC is maintained until the hard stop-layer is reached at which time a constant thickness FCP is produced on the stop-layer. However, even with this pulse-periodic continuous etching, there is some statistical variation in the etched surface, best seen by the side of the feature for Cycle 36. A longer overetch would be required to remove these patches of residual SiO_2. (Overetch refers to additional etching time after the stop-layer is initially cleared.)

With $T_p = 20$ s, the thicker FCP layer is not fully removed following an etch cycle—and this removal of the FCP is statistical. That is, the remaining FCP at the end of the etch step is thicker at some locations than others. For moderately short values of T_i, the locally thicker FCP layer translates to a lower EPC at that location for the next etch cycle and less fractional FCP removal during the etch step. This leaves an even locally thicker FCP at that location, which reduces the EPC the next cycle. The end result is a macroscopically rough etch front, which is unstable. Regions that have had high EPC due to being able to clear the FCP the prior cycle continue to etch rapidly. Regions that have had a low EPC due to not being able to remove a thick FCP layer are faced with even thicker FCP that slows EPC the next cycle.

The average thicknesses of the FCP layer and of the fluorocarbon-SiO_2 interfacial complex are shown in Fig. 9 during

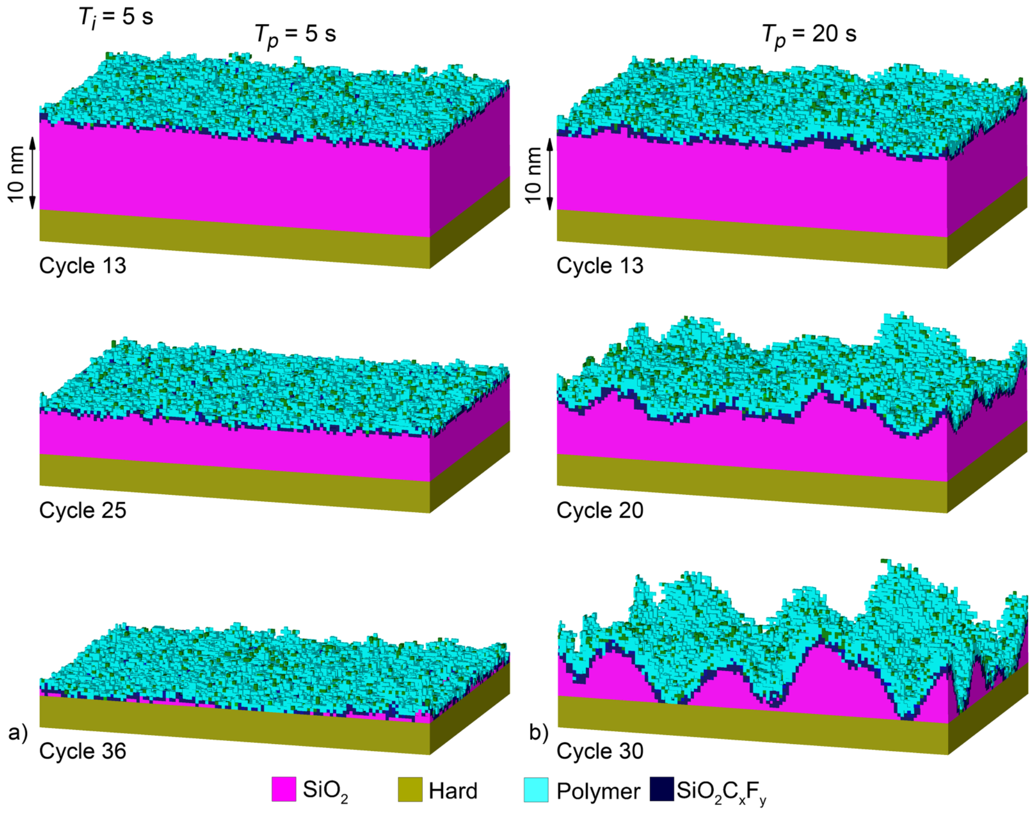

FIG. 8. Evolution of blanket SiO_2 features for ion sputtering time $T_i = 5$ s and passivation times of (a) $T_p = 5$ s and (b) $T_p = 20$ s. The longer T_p produces an increasingly rough surface.

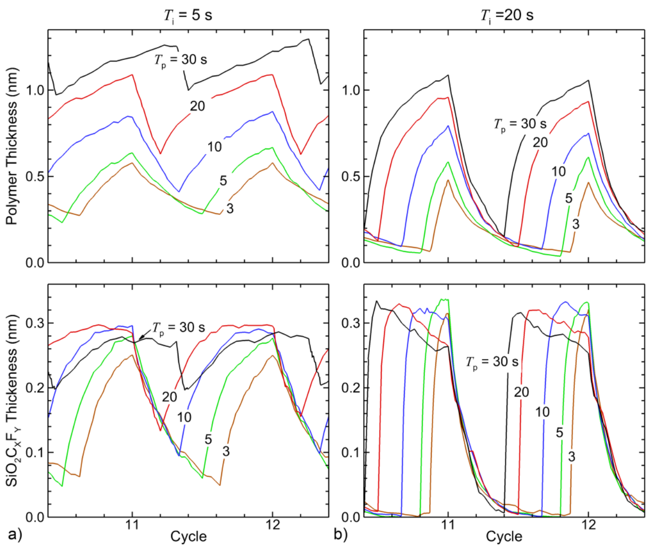

FIG. 9. ALE properties for (a) $T_i = 5$ s and (b) $T_i = 20$ s for different passivation times T_p during ALE cycles 9–12. The actual time per cycle is the sum of T_i and T_p while not accounting for pump-out and gas injection times. The thickness of the polymer is shown in the top frame and the thickness of the passivation layer $SiO_2C_xF_y$ in the bottom frame.

two ALE cycles for $T_i = 5$ and 20 s. Values are shown for different passivation times, T_p. The time scale is normalized by the time per cycle, so each T_p curve corresponds to a different real time. With the shorter T_i, the thickness of both the FCP (up to 1.2 nm) and the interfacial complex (up to 0.3 nm) increase with increasing T_p, leading to a reduction in EPC and eventual etch-stop. For $T_i = 20$ s, the fluorocarbon-SiO_2 interfacial complex is essentially completely removed at the end of the etch cycle, with there being only statistical instances of FCP left on the surface. The interfacial complex is rapidly replenished from the bare SiO_2 with the start of the next passivation cycle. With increasing T_p, the maximum thickness of the interfacial complex remains constant at 0.3 nm during the deposition period, while the total thickness of the FCP layer continues to increase up to 1.1 nm for $T_p = 30$ s. The residual thickness of the FCP at the end of the etch step also increases with increases in T_p. However, the layer remains thin enough to allow ion penetration and activation of etching at the interface.

Although the qualitative trends just discussed apply to a wide range of operating conditions, the quantitative trends depend on the details of the operating conditions. For example, increasing the flow rate of C_4F_8 in the gas mixture by a factor of 2 (from $Ar/C_4F_8/O_2 = 95/4/1$ with total flow rate of 800 SCCM to $Ar/C_4F_8/O_2 = 91/8/1$) increases the fluorocarbon radical flux to the substrate from 1.43×10^{16} to $2.03 \times 10^{16}\ cm^{-2}\ s^{-1}$. The thickness of the FCP after 50 s of continuous deposition is 0.8 nm for C_4F_8 flow rate of 20 SCCM and 2.4 nm for a flow rate of 40 SCCM.

With the higher fluorocarbon radical flux and with there being only a nominal change in the ion flux, the ALE window for continuous etching is considerably narrower. For example, EPC as a function of passivation time T_p for different etch times T_i (1, 5, 10, 20, and 30 s) are shown in Fig. 10 for the higher flow rate of C_4F_8. The height of the surface is also shown with $T_i = 10$ s for T_p values from 1 to 30 s. The square symbols on the EPC curves in Fig. 10(a) separate conditions producing smooth, continuously etching surfaces (smaller T_p) from roughening surfaces (larger T_p). With the higher fluorocarbon radical fluxes, continuous smooth etching can only be achieved for shorter values of T_p, no longer than $T_p = 15$ s, while requiring longer T_i to clear the thickening FCP layer. For $T_i = 10$ s, continuous etching to the stop-layer is only achieved with $T_p < 3$ s. Longer deposition times are able to

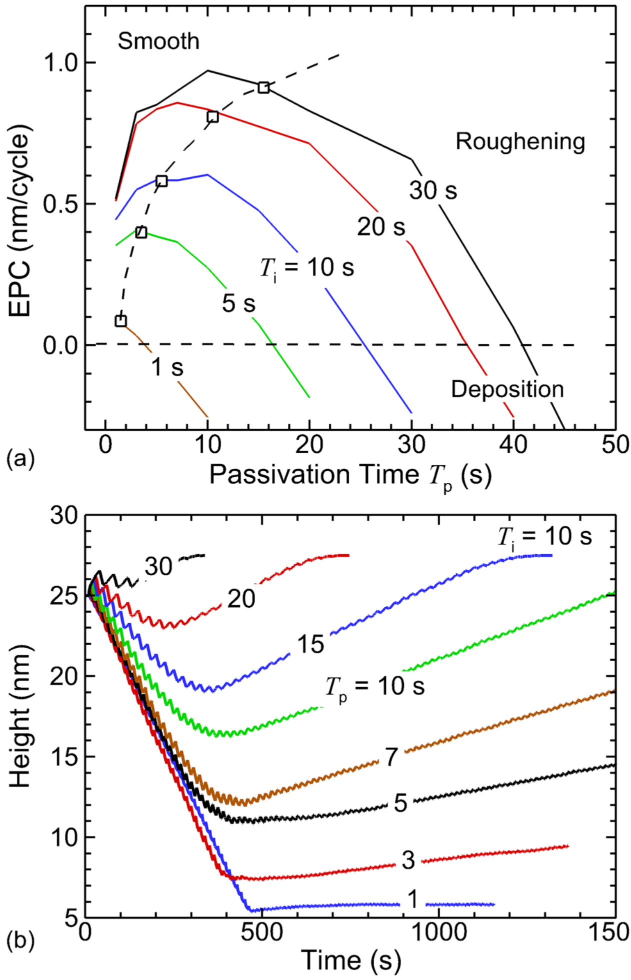

FIG. 10. ALE properties when doubling the C_4F_8 flow rate in the $Ar/C_4F_8/O_2$ mixture above the base case. (a) EPC as a function of T_p, for $T_i = 1$, 5, 10, 20, and 30 s. The symbol on each curve is the transition between smooth continuous etching (lower T_p) and roughening (higher T_p) surfaces. (b) Evolution of etch front height as a function of time with $T_i = 10$ s and $T_p = 1$, 3, 5, 7, 10, 15, 20, and 30 s.

sustain shorter periods of continuous etching before the FCP thickens to the point that etching ends and FCP deposition dominates.

The roughening of the surface due to statistical thickening of the FCP layer may occur for different reasons in two ion energy regimes. In low ion energy regimes, EPC is limited by the ability of ions to penetrate through the FCP. Statistically thicker FCP then translates to locally lower EPC, which leads to roughening. In high ion energy regimes, the EPC is limited by the availability of the FCP, which serves as the fuel for chemical sputtering. Statistically thicker FCP then translates to locally higher EPC provided the ion penetration distance exceeds the statistical FCP thickness. The locally higher EPC then leads to roughening. In either regime, statistical variation in the FCP thickness can produce spatially dependent EPC, leading to roughening.

These results suggest three etching modes for ALE of dielectrics in fluorocarbon plasmas. Features demonstrating these three modes before and after cleaning the FCP from the feature are shown in Fig. 11. (The "cleaning" of polymer consists of removing the computational cells occupied by polymer to reveal the underlying SiO_2. So this would be perfect cleaning. We do not simulate a cleaning process that might affect the surface roughness.) These features are shown at the time of an etch-stop or when the etch is completed. In mode 1 ($T_p = 30$ s), etching either does not start or ends after only a few cycles. The ion bombardment time T_i is either too short (or T_p is too long) to fully remove the FCP layer at the end of each cycle. The thickness of the FCP layer quickly increases to above the penetration distance of the incident ions. The end result is a pure deposition regime while retaining a smooth surface. In mode 2 ($T_p = 10$ s), having longer T_i or shorter T_p enables continuous etching to proceed for some period of time, after which an etch-stop may occur. In this mode, the ion penetration distance through the FCP exceeds its thickness; however, the FCP is not fully removed in each cycle. A small buildup of polymer occurs with each cycle until an etch-stop occurs. As the FCP thickness increases, its removal becomes more statistical, producing a spatial variation in FCP thickness and so a spatial variation in EPC that roughens the surface. In mode 3 ($T_p = 1$ s), continuous etching can be sustained indefinitely, as the FCP is fully removed during each cycle. The surface remains smooth.

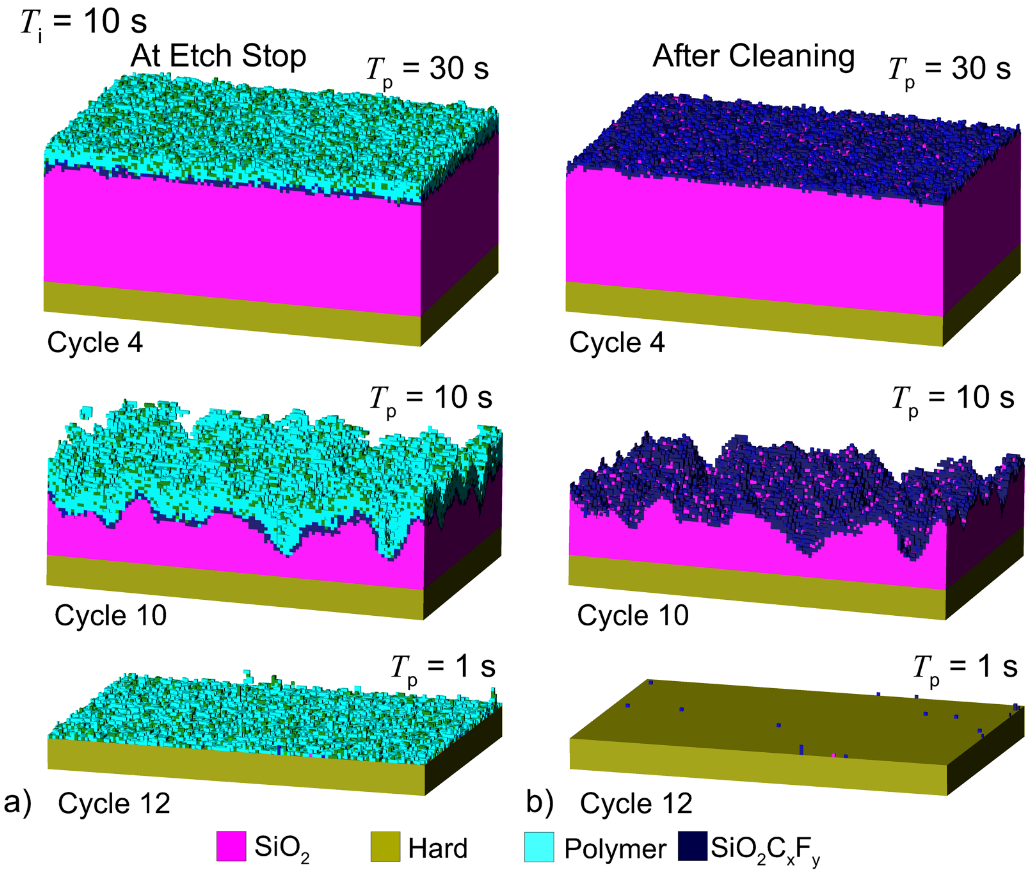

FIG. 11. ALE of blanket SiO_2 for $T_i = 10$ s, and passivation times of $T_p = 30$, 10, and 1 s. Images are shown at the time of etch-stop (or when the feature is cleared) (a) with polymer and (b) with polymer removed.

C. Consequences of low frequency power

The voltage magnitude of the low frequency (LF) bias during the etching phase largely controls the ion energy incident onto the wafer, with a secondary influence on the magnitude of ion fluxes. For a given T_i, higher ion fluxes will enable more polymer to be utilized in etching the underlying SiO_2, thereby enabling larger EPC. Higher ion fluxes will also clear more FCP from the surface, leading to a less statistical FCP thickness and smoother films. Higher ion energies enable a longer penetration distance through the FCP, and so are more tolerant of thicker FCP layers.

The LF bias power for the dual-frequency CCP plasma used for the etch step was varied from 30 to 200 W. With the ionization being dominated by the high frequency power, the sevenfold increase in LF power produced less than a twofold increase in peak electron density, from 2.9×10^{10} to $5.0 \times 10^{10}\ \mathrm{cm}^{-3}$. Ion fluxes at midradius of the wafer increased from $1.5 \times 10^{15}\ \mathrm{cm}^{-2}\,\mathrm{s}^{-1}$ for 30 W to $2.5 \times 10^{15}\ \mathrm{cm}^{-2}\,\mathrm{s}^{-1}$ for 200 W. The IEADs for these conditions are shown in Fig. 12. The maximum ion energy increased from about 100 eV at 30 W to about 290 eV at 200 W, with the self-DC bias decreasing from −68.9 to −213 V. The angular width of the IEAD narrows from ±6° at 30 W to ±3° at 200 W.

The EPC as a function of LF bias power is shown in Fig. 13(a) as a function of passivation time T_p for $T_i = 20$ s. For LF bias powers of less than 50 W, continuous etching can only be sustained for a limited range of short passivation times. For example, for an LF bias power of 30 W, the EPC increases to 0.7 nm/cycle with an increase of passivation time to 6 s. For longer passivation times, the polymer removal each cycle is not complete, leading to a cycle-to-cycle increase in polymer thickness until the incident ions are no longer able to penetrate the polymer to the etch front. At this time, the system transitions to pure polymer deposition. For LF bias powers above 50 W, the system largely remains in a continuous etch mode for passivation times of up to 40 s. Although there is a factor of 2 increase in ion flux from 30 to 200 W, the increase in EPC and the ability to continuously sustain that increase is largely

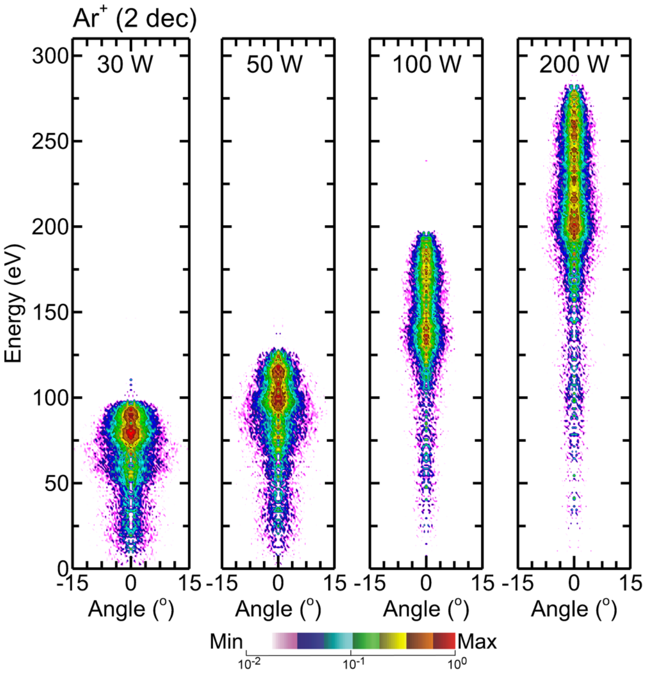

FIG. 12. IEAD of Ar$^+$ to the wafer for LF powers of 30, 50, 100, and 200 W in the dual-frequency CCP Ar discharge plotted on a log scale over two decades.

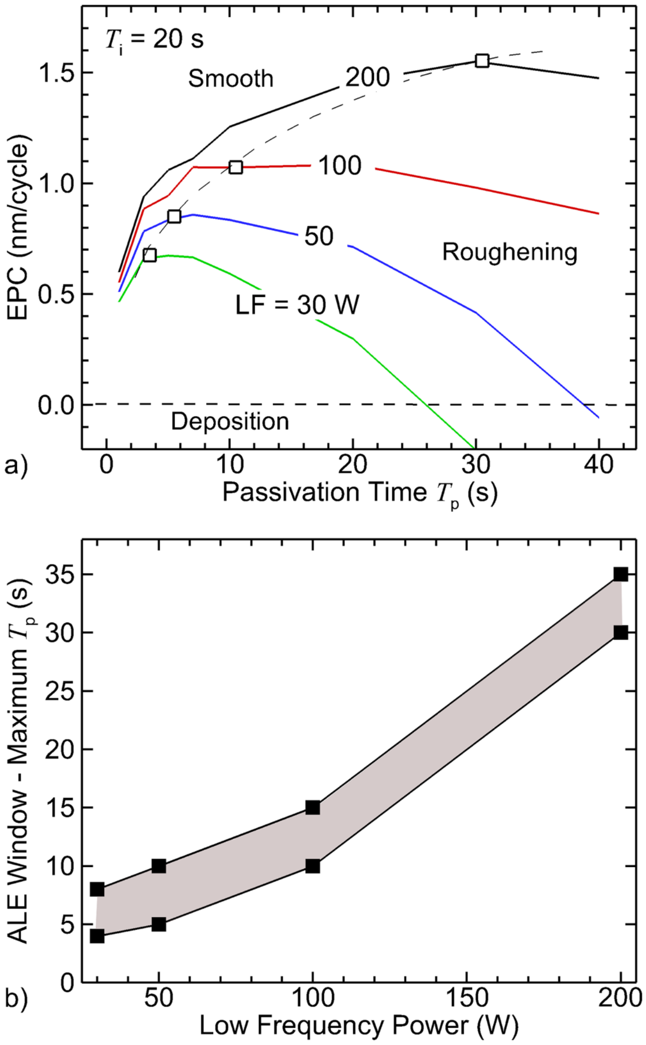

FIG. 13. ALE characteristics for LF power. (a) EPC for $T_i = 20$ s as a function of passivation time T_p for different LF powers of 30, 50, 100, and 200 W during the ion sputtering step. The symbol on each curve is the transition between smooth continuous etching (lower T_p) and roughening surfaces (higher T_p). (b) ALE window as a function of LF power. The ALE window is expressed as the range of T_p *below* which smooth, consistent cycle-to-cycle etching occurs (though not necessarily an EPC of 1 monolayer/cycle).

due to the increase in ion energy. The higher ion energies enable penetration through a thickening FCP layer while also sputtering some of that FCP. The maximum EPC increases with increasing LF power (0.7 nm/cycle at 30 W to 1.6 nm/cycle at 200 W). The maxima in EPC with increasing LF power occur at successively longer passivation times as the more energetic ions are able to penetrate and utilize thicker FCP layers.

The etch profiles for LF biases of 30, 100, and 200 W are shown in Fig. 14 for $T_i = 20$ s and $T_p = 30$ s. Profiles are shown during the active ALE cycles and at the time that either an etch-stop occurs or the stop-layer is reached. For an LF bias of 30 W, continuous etching can only be sustained up to a passivation time of $T_p = 25$ s. With $T_p = 30$ s, the cycle-to-cycle increase in FCP layer thickness exceeds the penetration depth of the incident ions, and there is a transition to pure deposition by the third or fourth cycle. With a LF bias of 100 W, continuous etching is barely sustainable. The average FCP layer remaining at the end of the etch step is less than a monolayer; however, there is statistical FCP residue left on the surface. The statistical residue leads to locally thicker patches of FCP, resulting in locally lower EPC for low energy ions (or higher EPC for high energy ions). The end result is a rough surface. In principle, this rough surface can be etched to smoothness at the stop-layer by performing a significant over-etch providing that the stop-layer is nonreactive. Achieving consistently smooth surfaces down to the stop-layer requires essentially complete removal of the FCP layers on each cycle, as produced with an LF bias of 200 W.

The ALE *window* refers to that range of operating conditions for which ideal-like ALE can be achieved.[1,43] Ideal ALE, at least for conductor etch in a nonpolymerizing system, would consist of no etching during the passivation portion of the cycle and one monolayer removed during the ion bombardment portion of the cycle. Definition of the ALE window in these systems is aided by both steps being self-limiting. The definition of the ALE window for dielectric etching in polymerizing systems is less clear due to the polymerizing step not being self-limiting. The ALE window

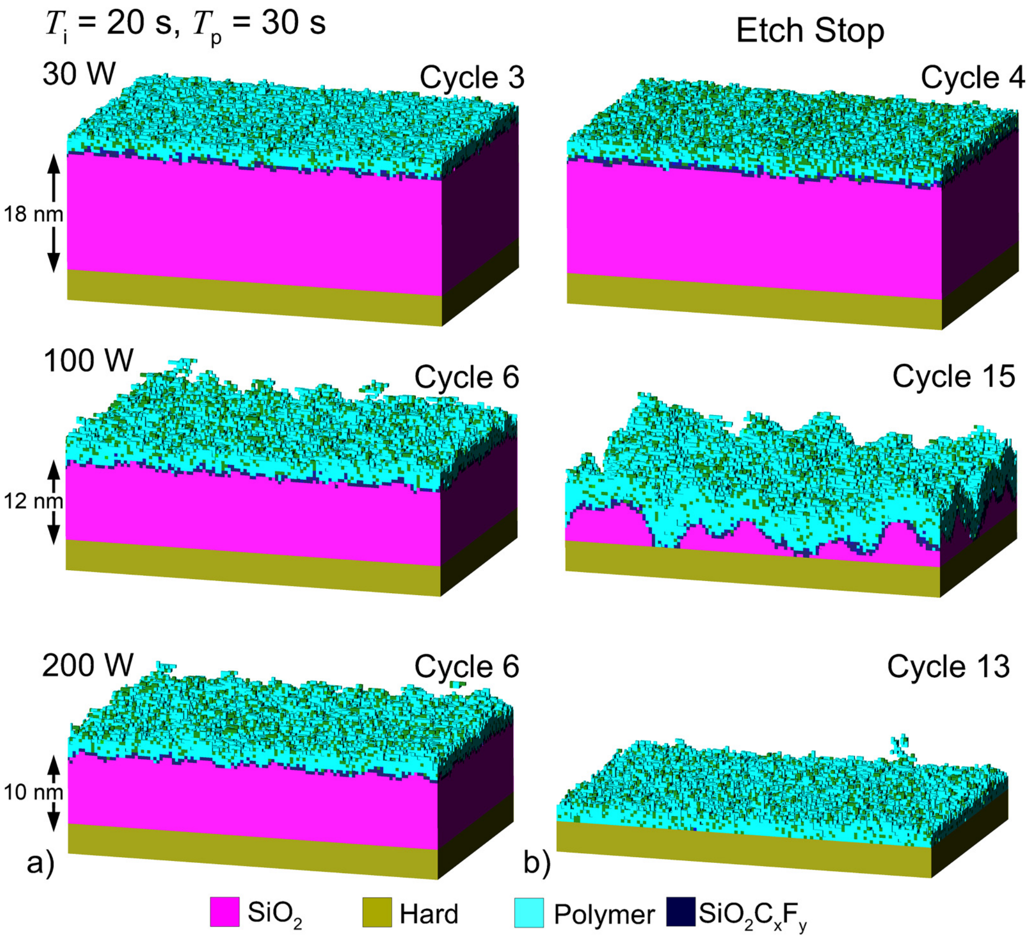

FIG. 14. Blanket SiO$_2$ surfaces during ALE with $T_i = 20$ s and $T_p = 30$ s for LF powers of 30, 100, and 200 W during the ion sputtering step. (a) Features after a selected number of cycles during quasicontinuous ALE. (b) Features at the time of etch-stop or when the feature is cleared.

might best be defined as a consistent cycle-to-cycle removal of material (not necessarily a single monolayer) with a smooth surface. Adopting that definition, the ALE window will be a function of T_i, T_p, and LF power. For example, for our simulated conditions, the ALE window is shown in Fig. 13(b) as a function of LF power with $T_i = 20$ s. The ALE window is defined in terms of the range of passivation times T_p below which smooth, consistent cycle-to-cycle etching occurs. A range of values for T_p is given as the assessment of smooth and consistent is somewhat qualitative. The ALE window broadens to larger T_p with increasing LF power as the increase in ion energy is able to utilize thicker FCP layers without leaving statistical patches of polymer that lead to roughening.

V. SHORT TRENCH ETCHING OF SiO_2

ALE of features, as opposed to blanking etching, have additional challenges related to the angular distribution of reactants, shadowing, and redeposition. These challenges are demonstrated by performing ALE in the feature shown in Fig. 15. This short trench feature is intended to represent the etching of a 20 nm thick dielectric ARC (antireflection coating) to open a window for a subsequent etch into the underlying material. The goal is to remove the dielectric ARC (here idealized as SiO_2) with straight walls to preserve the pattern of the perfect PR mask, 50 nm tall. The short trench has dimensions of $20 \times 40\ \mathrm{nm}^2$.

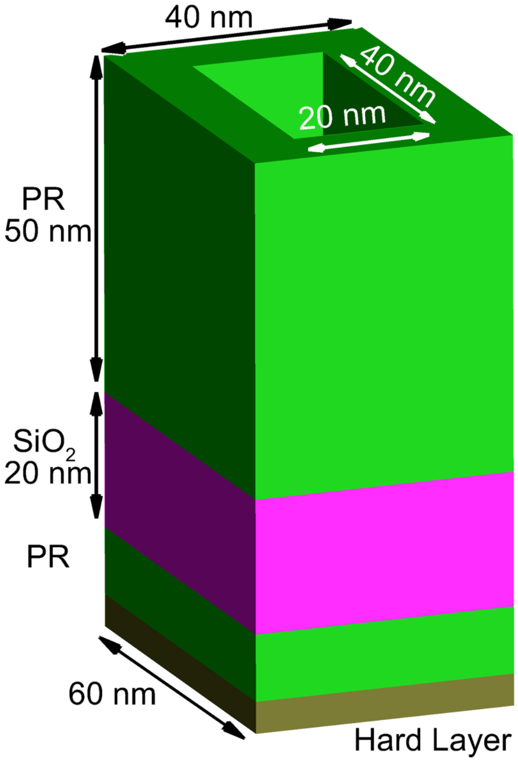

FIG. 15. Schematic of the short trench feature prior to etching, having a height of PR of 50 nm over a 20 nm thick ARC (SiO_2).

Side cut views of the trenches at the level of the ARC are shown in Fig. 16 during ALE with an LF bias power of 50 W, sputtering time of $T_\mathrm{i} = 30$ s, and passivation times of $T_\mathrm{p} = 2$, 5, 10, and 30 s. Profiles are shown in Fig. 16(a), with the polymer retained, at the time that the feature stops evolving or when an etch-stop is reached. The same features with the polymer removed are shown in Fig. 16(b). The results are labeled with two cycle numbers. The first is the number of cycles required to reach the bottom stop-layer. The second is the number of cycles when the feature stops evolving. The difference between the two values is the number of overetch cycles (e.g., 17 overetch cycles for $T_\mathrm{p} = 2$ s and 7 overetch cycles for $T_\mathrm{p} = 10$ s). The feature stops evolving when the polymer has thickened in excess of what can be removed during each cycle and thickened beyond the penetration depth of the ions. The etch sequence is shown in Fig. 16(c) for $T_\mathrm{p} = 5$ s with the polymer retained. The cycles for this figure were chosen to best illustrate the evolution of the feature.

With increasing T_p, the thickness of the FCP increases on the sidewalls as well as on the bottom of the feature. At the time at which the feature stops evolving, the sidewall polymer thickness at the top of the ARC is 1.5 nm for $T_\mathrm{p} = 2$ s, 2.7 nm for $T_\mathrm{p} = 5$ s, 4.2 nm for $T_\mathrm{p} = 10$ s, and 4.8 nm for $T_\mathrm{p} = 30$ s. The thicker sidewall passivation leads to tapering of the feature and, for $T_\mathrm{p} = 30$ s, an etch-stop. The thickness of the sidewall passivation increases with successive ALE cycles, which leads to an decreasing sidewall slope, as shown in Fig. 16(c). The overetch for $T_\mathrm{p} = 5$ s is able to improve the sidewall slope to some degree before the etch-stop occurs, but this is a nominal effect (see the discussion below). Note that there is a vestige of ARC remaining on the bottom of the feature for $T_\mathrm{p} = 10$ s. This vestige of ARC is a consequence of the statistical variation in the thickness of the FCP, which at that location happened to be thicker than the ion penetration depth. With the cessation of etching of the ARC, the consumption of polymer by the etching process ends, and the FCP thickness rapidly increases. All features then eventually fill with polymer if the ALE cycles continue.

The quality of the final feature, with vertical walls being desired, is partly determined by the thickness of the FCP and the ability of incident ions to either penetrate or sputter the polymer. Trench profiles in the vicinity of the ARC for LF bias powers of 30–200 W are shown in Fig. 17 for a sputtering time of $T_\mathrm{i} = 30$ s and a passivation time of $T_\mathrm{p} = 10$ s. As in Fig. 16, the number of ALE cycles to first reach the ARC and number of cycles when the feature stops evolving are noted. The images show the features at the end of profile evolution with polymer [Fig. 17(a)] and with polymer removed [Fig. 17(b)]. The evolution with ALE cycles of the feature for 200 W with polymer removed is also shown in Fig. 17(c). (The cycles for this figure were chosen to best illustrate the evolution of the feature.) The slope of the sidewalls and polymer thickness decrease with increasing LF power. At the end of profile evolution, the sidewall polymer is 5 nm thick for 30 W, decreasing to 1.7 nm thick for 200 W. Since the fluence of fluorocarbon radicals is nearly independent of LF bias power, the decrease in the thickness of the FCP is largely due to increased sputtering of the polymer. For these process conditions, straight

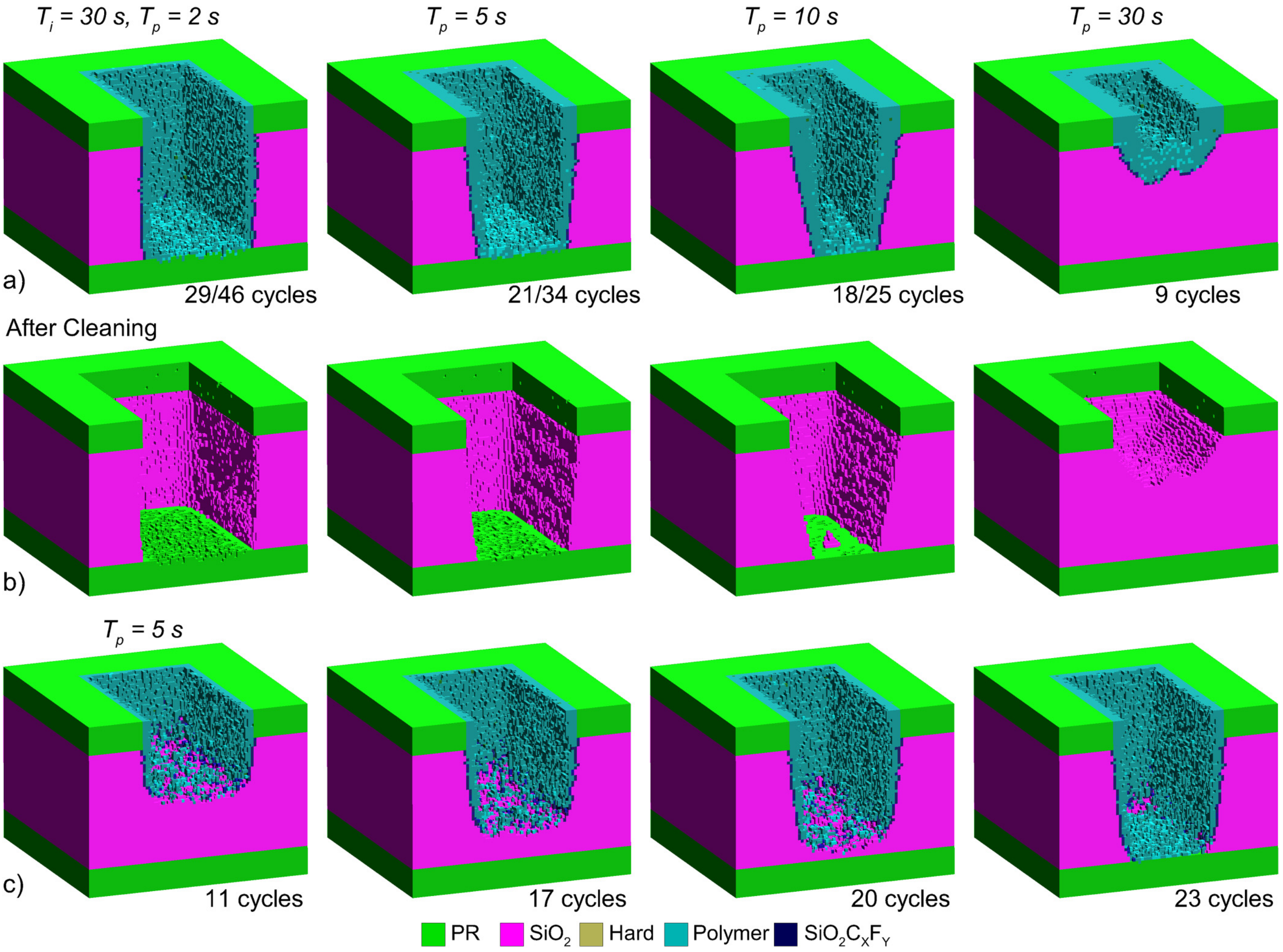

FIG. 16. Side cut view of the trench profiles in the vicinity of the ARC for $T_i = 30$ s and $T_p = 2$, 5, 10, and 30 s. (a) The time at which the feature stops evolving. The notation for cycles, for example, 29/48, indicates that the feature reaches the stop-layer after 29 cycles and the feature stops evolving after 48 cycles—an overetch of 19 cycles. (b) Same features but with polymer removed. (c) Time evolution of the feature with $T_p = 5$ s after 11, 17, 20, and 23 cycles with the polymer retained. The final feature after 34 cycles is shown in (b).

sidewalls are only achieved with an LF power of 200 W, though the increase in bias power also initiates physical sputtering of the top of the PR (not shown) and on the bottom of the feature.

The number of overetch cycles required to completely evolve the feature decreases with increasing LF power—nine cycles at 30 W to four cycles at 200 W. At the lower powers, the FCP thickness incrementally increases with each ALE cycle, which decreases the EPC, which then extends the number of cycles required for overetch. For a LF power of 200 W, the FCP thickness is nearly constant cycle-to-cycle, thereby enabling a more efficient overetch requiring a smaller number of cycles.

In conventional high-aspect-ratio (HAR) etching in CCPs, the ion energies can be as high as several keV and while the polymer is thin (<1 nm). As a result, the sidewall slope of the feature continues to evolve during the overetch. Etching can proceed even at glancing angles by these high energy ions. The sidewall typically becomes more vertical, and in some cases transitions to bowing, during overetch. In contrast, these simulated ALE results indicate that as the feature is cleared and overetch begins, there is no significant change in the sidewall slope. The overetch serves only to clear the bottom corners of the feature. We ascribe this behavior to the low ion energies and relatively thick polymer. Once the polymer on the sidewalls has thickened to the point that etching is terminated at that height, then the sidewall slope will not change. The low energy, glancing incidence ions simply do not have enough energy to penetrate the polymer to continue to evolve the sidewall slope.

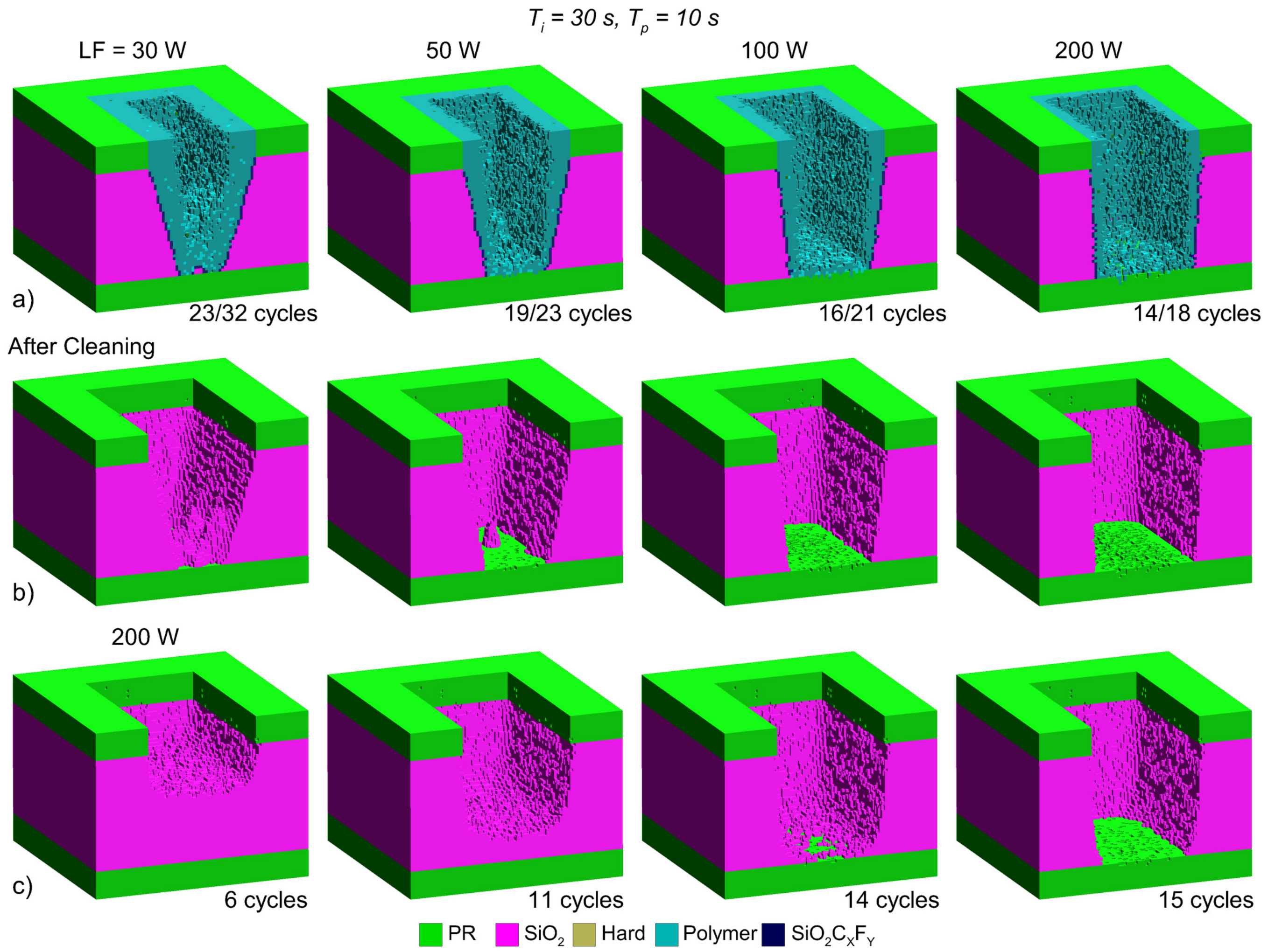

FIG. 17. Side cut view of the trench profiles in the vicinity of the ARC for $T_i = 30$ s and $T_p = 10$ s for LF power during sputtering of 30, 50. 100, and 200 W. (a) The time at which the feature stops evolving. The notation for cycles, for example, 23/32, indicates that the feature reaches the stop-layer after 23 cycles and the feature stops evolving after 32 cycles—an overetch of 9 cycles. (b) Same features but with polymer removed. (c) Time evolution of the feature for 200 W after 6, 11, 14, and 25 cycles with polymer removed. The final feature after 18 cycles is shown in (b).

These trends place added value on achieving the desired sidewall slope from the start of the etch as the slope will not greatly evolve during the overetch.

VI. CONCLUDING REMARKS

ALE of dielectrics using fluorocarbon gas mixtures by cyclic passivation and sputtering steps provides the ability to control the etch rate and feature fidelity, while being sensitive to polymer thickness (passivation) and ion energy distributions (sputtering). Scaling of ALE of blanket and short trench SiO_2 by controlling the thickness of polymer and sputtering ion energies was computationally investigated. The ALE process is sensitive to the initial FCP thickness at the start of the chemical sputtering step, which can be controlled by gas mixture and passivation time T_p. Thinner FCP layers allow ions to penetrate into the interface between the FCP and SiO_2 to activate etching. As long as the ions have this penetrating ability, EPC increases with increasing passivation time T_p as there is additional polymer *fuel* to react with the SiO_2. In this regard, a thin FCP layer enables a stable pulse-periodic steady-state ALE, with SiO_2 being continually etched.

For a given length of the chemical sputtering step, T_i, thicker FCP layers produced during passivation can be utilized by increasing the ion energy. For a given ion energy, the process dependence on sputtering time T_i is less clear. If the ion energy is not high enough to penetrate to the FCP-SiO_2 interface, etching will not occur at the start of the chemical sputtering step. However, if the ion energy is high enough to sputter the polymer, lengthening T_i will reduce the FCP thickness until ions can penetrate into the interface. At this later time in the cycle, etching will begin.

If the polymer is not fully removed after each chemical sputtering cycle, the residual polymer will incrementally contribute to the FCP thickness produced during the next passivation step. The thickening FCP will eventually exceed the penetration depth of ions during chemical sputtering, and etching will stop. That is, the EPC is transient and cycle dependent. Due to the statistical nature of both polymer removal and etching, there may be spots of residual polymer that remain at the end of the chemical sputtering portion of the cycle. These random spots of polymer result in locally thicker FCP layers following the next cycle of passivation. The thicker FCP generally produces a lower than average EPC for low energy ions (ion energy limited) or higher than average EPC for high energy ions (FCP thickness limited). In either case, the spatially dependent EPC can then lead to roughening of the surface.

These trends motivate classifying plasma ALE of dielectrics in fluorocarbon plasmas into three modes of operation: smooth surface with continuous etching, roughening surface with eventual etch-stop, and pure deposition. For a given set of passivating and chemical sputtering fluxes, these modes are determined by combinations of passivation time T_{i} and sputtering time T_{i}. In all cases, increasing bias power and ion energies during the chemical sputtering phase generally increases the operational space in which continuous ALE with smooth surfaces can be achieved, which provides a larger ALE window. As long as ion energies are low enough to maintain selectivity and prevent physical sputtering, there are generally benefits to increasing ion energy.

For the same conditions as blanket etching, the operational window for ALE of trenches is significantly narrower. This narrower operational window in large part results from the generally thicker FCP on sidewalls due to ions having grazing incident angles. Ions with grazing incidence angles have a lower polymer sputtering probability and longer path length through the FCP. These conditions inherently lead to sidewall slopes, which must be straightened by overetch periods. However, the ability to straighten the sidewalls and complete the overetch is in competition with the thickening FCP on the sidewalls that occurs during overetch. Unlike conventional HAR etching, there is limited ability to change the sidewall slope during the overetch. The thickening FCP on the sidewalls will eventually fill (or *clog*) the feature. These conditions also prevail during continuous, conventional etching. In conventional etching, increasing ion energy typically can overcome these limitations. However, during ALE, there is an upper limit to the ion energy for which the desired characteristics of ALE are maintained—that is, ion energies should be below the physical sputtering threshold. As a result, ALE is more sensitive to the competition between overetch and thickening FCP layers on the sidewalls.

DATA AVAILABILITY

The data that support the findings of this study are available from the corresponding author upon reasonable request.

ACKNOWLEDGMENTS

This work was supported by Tokyo Electron Inc. and the National Science Foundation (No. PHY-2009219). This material was also based on the work supported by the U.S. Department of Energy, Office of Sciences, under Award Nos. DE-SC000319 and DE-SC0020232.

REFERENCES

[1] K. J. Kanarik, T. Lill, E. A. Hudson, S. Sriraman, S. Tan, J. Marks, V. Vahedi, and R. A. Gottscho, J. Vac. Sci. Technol. A **33**, 020802 (2015).

[2] V. M. Donnelly and A. Kornblit, J. Vac. Sci. Technol. A **31**, 050825 (2013).

[3] H. Abe, M. Yoneda, and N. Fujiwara, Jpn. J. Appl. Phys. **47**, 1435 (2008).

[4] C. G. N. Lee, K. J. Kanarik, and R. A. Gottscho, J. Phys. D: Appl. Phys. **47**, 273001 (2014).

[5] K. J. Kuhn *et al.*, *International Electron Devices Meeting*, San Francisco, CA, 2012 (IEEE, San Francisco, 2012), pp. 8.1.1–8.1.4.

[6] S. J. Fonash, IBM J. Res. Dev. **43**, 103 (1999).

[7] S. D. Kim, J. J. Lee, S. H. Lim, and H. J. Kim, J. Appl. Phys. **85**, 5992 (1999).

[8] S. J. Fonash, C. R. Viswanathan, and Y. D. Chan, Solid State Technol. **37**, 99 (1994).

[9] N. Yabumoto, M. Oshima, O. Michikami, and S. Yoshii, Jpn. J. Appl. Phys. **20**, 893 (1981).

[10] N. Kuboi, T. Tatsumi, T. Kinoshita, T. Shigetoshi, M. Fukasawa, J. Komachi, and H. Ansai, J. Vac. Sci. Technol. A **33**, 061308 (2015). .

[11] K. Eriguchi and K. Ono, J. Phys. D: Appl. Phys. **41**, 024002 (2008).

[12] K. Eriguchi, Y. Nakakubo, A. Matsuda, Y. Takao, and K. Ono, IEEE Electron Device Lett. **30**, 1275 (2009).

[13] K. J. Kanarik, T. Lill, E. A. Hudson, S. Sriraman, S. Tan, J. Marks, V. Vahedi, and R. A. Gottscho, J. Vac. Sci. Technol. A **35**, 05C302 (2017).

[14] C. T. Carver, J. J. Plombon, P. E. Romero, S. Suri, T. A. Tronic, R. B. Turkot, ECS J Solid State Sci. Technol. **4**, N5005 (2015).

[15] G. S. Oehrlein, D. Metzler, and C. Li, ECS J Solid State Sci. Technol. **4**, N5041 (2015).

[16] H. Sakaue, S. Iseda, K. Asami, J. Yamamoto, M. Hirose, and Y. Horiike, Jpn. J. Appl. Phys. **29**, 2648 (1990). .

[17] S. D. Athavale and D. J. Economou, J. Vac. Sci. Technol. B **14**, 3702 (1996).

[18] A. Ludviksson, M. Xu, and R. M. Martin, Surf. Sci. **277**, 282 (1992).

[19] J. C. Patrin, Y. Z. Li, M. Chander, and J. H. Weaver, Appl. Phys. Lett. **62**, 1277 (1993).

[20] T. Matsuura, J. Murota, Y. Sawada, and T. Ohmi, Appl. Phys. Lett. **63**, 2803 (1993).

[21] S. Imai, T. Haga, O. Matsuzaki, T. Hattori, and M. Matsumura, Jpn. J. Appl. Phys. **34**, 5049 (1995).

[22] S. -D. Park, K. -S. Min, B. -Y. Yoon, D. -H. Lee, and G. -Y. Yeom, Jpn. J. Appl. Phys. **44**, 389 (2005). .

[23] S. D. Athavale and D. J. Economou, J. Vac. Sci. Technol. A **13**, 966 (1995).

[24] C. M. Huard, S. J. Lanham, and M. J. Kushner, J. Phys. D: Appl. Phys. **51**, 155201 (2018).

[25] Y. I. Jhon, K. S. Min, G. Y. Yeom, and Y. M. Jhon, Appl. Phys. Lett. **105**, 093104 (2014).

[26] K.-Y. Lin, C. Li, S. Engelmann, R. L. Bruce, E. A. Joseph, D. Metzler, and G. S. Oehrlein, J. Vac. Sci. Technol. A **36**, 040601 (2018).

[27] A. Agarwal and M. J. Kushner, J. Vac. Sci. Technol. A **27**, 37 (2009).

[28] D. Metzler, R. L. Bruce, S. Engelmann, E. A. Joseph, and G. S. Oehrlein, J. Vac. Sci. Technol. A **32**, 020603 (2014).

[29] M. Wang, P. L. G. Ventzek, and A. Ranjan, J. Vac. Sci. Technol. A **35**, 031301 (2017).

[30] D. Metzler, C. Li, S. Engelmann, R. L. Bruce, E. A. Joseph, and G. S. Oehrlein, J. Chem. Phys. **146**, 052801 (2017).

[31] C. Li, D. Metzler, C. S. Lai, E. A. Hudson, and G. S. Oehrlein, J. Vac. Sci. Technol. A **34**, 041307 (2016).

[32] C. M. Huard, S. Sriraman, A. Paterson, and M. J. Kushner, J. Vac. Sci. Technol. A **36**, 06B101 (2018).

[33] K.-Y. Lin, C. Li, S. Engelmann, R. L. Bruce, E. A. Joseph, D. Metzler, and G. S. Oehrlein, J. Vac. Sci. Technol. A **38**, 032601 (2020).

[34] S. Dallorto, A. Goodyear, M. Cooke, J. E. Szornel, C. Ward, C. Kastl, A. Schwartzberg, I. W. Rangelow, and S. Cabrini, Plasma Processes Polym. **16**, e1900051 (2019).

[35] T. Tsutsumi, H. Kondo, M. Hori, M. Zaitsu, A. Kobayashi, T. Nozawa, and N. Kobayashi, J. Vac. Sci. Technol. A **35**, 01A103 (2017).

[36] A. Pranda, K.-Y. Lin, S. Engelmann, R. L. Bruce, E. A. Joseph, D. Metzler, and G. S. Oehrlein, J. Vac. Sci. Technol. A **38**, 052601 (2020).

[37] R. J. Gasvoda, Y. G. P. Verstappen, S. Wang, E. A. Hudson, and S. Agarwal, J. Vac. Sci. Technol. A **37**, 051003 (2019).

[38] Y. Cho, Y. Kim, S. Kim, and H. Chae, J. Vac. Sci. Technol. A **38**, 022604 (2020).

[39] M. J. Kushner, J. Phys. D: Appl. Phys. **42**, 194013 (2009).

[40] A. V. Vasenkov, X. Li, G. S. Oehrlein, and M. J. Kushner, J. Vac. Sci. Technol. A **22**, 511 (2004).

[41] A. Sankaran and M. J. Kushner, J. Vac. Sci. Technol. A **22**, 1242 (2004).

[42] M. Kawakami, D. Metzler, C. Li, and G. S. Oehrlein, J. Vac. Sci. Technol. A **34**, 040603 (2016).

[43] K. J. Kanarik, S. Tan, W. Yang, I. L. Berry, Y. Pan, and R. A. Gottscho, J. Vac. Sci. Technol. A **39**, 010401 (2021).